Morphological Evolution of Tin Oxide Nanobelts after Phase Transition

ARTICLE *in* CRYSTAL GROWTH & DESIGN · FEBRUARY 2008

Impact Factor: 4.89 · DOI: 10.1021/cg7009379

4 AUTHORS:

Marcelo Ornaghi Orlandi
São Paulo State University
62 PUBLICATIONS **1,002** CITATIONS
SEE PROFILE

Antonio J Ramirez
The Ohio State University
124 PUBLICATIONS **985** CITATIONS
SEE PROFILE

Edson R. Leite
Universidade Federal de São Carlos
522 PUBLICATIONS **9,209** CITATIONS
SEE PROFILE

Elson Longo
São Paulo State University
882 PUBLICATIONS **15,087** CITATIONS
SEE PROFILE

CRYSTAL GROWTH & DESIGN
2008
VOL. 8, NO. 3
1067–1072

Morphological Evolution of Tin Oxide Nanobelts after Phase Transition

Marcelo Ornaghi Orlandi,*,† Antonio José Ramirez,‡ Edson Roberto Leite,§ and Elson Longo△

Departamento de Física e Química, Universidade Estadual Paulista, CEP 15385-000, P.O. Box 31, Ilha Solteira-SP, Brazil, Laboratório Nacional de Luz Síncrotron (LNLS), Campinas-SP, Brazil, Departamento de Química, Universidade Federal de São Carlos, São Carlos-SP, Brazil, and Instituto de Química, Universidade Estadual Paulista, Araraquara-SP, Brazil

Received September 25, 2007; Revised Manuscript Received November 9, 2007

ABSTRACT: This article reports a study of the thermal stability and morphological changes in tin oxide nanobelts grown in the orthorhombic SnO phase. The nanobelts were heat-treated in a differential scanning calorimetry (DSC) furnace at 800 °C for 1 h in argon, oxygen, or synthetic air atmospheres. The samples were then characterized by DSC, X-ray diffraction (XRD), high resolution transmission electron microscopy (HRTEM), and high resolution field emission scanning electron microscopy (FE-SEM). The results confirmed that the orthorhombic SnO phase is thermodynamically unstable, causing the belts to transform into the SnO_2 phase when heat-treated. During the phase transition, if oxygen is available in the furnace atmosphere, nanofibers grow at the edge of nanobelts at about 50° of the belts' growth direction, while particles grow on the belt surface in the absence of oxygen. Although the decomposition process reduces the nanobelt cell volume by 22%, most belts remain monocrystalline after the heat treatment. The results confirm that phase transition is a decomposition process, which explains the morphological changes in the belts based on metallic tin generated in the process.

Introduction

Nanostructured materials are interesting due to their new or superior properties, allowing current theories to be tested or modified. A fundamental requirement for their application is maintaining control over their size, morphology, and chemical composition; ergo a wide range of approaches have been used to attain such characteristics.[1–7]

Wide band gap materials, such as tin oxide, present a combination of very attractive chemical, electronic, and optical properties, hence offering a wide variety of potential applications that include optoelectronic devices, gas sensors, catalysts, and photovoltaic cells;[8–11] moreover, SnO_2 nanobelts have been synthesized successfully by different routes.[12–14] In addition to tin dioxide nanobelts, tin monoxide discs,[15] nanobelts,[16,17] and thin films[18] have been recently reported, and studies pointed out that SnO has p-type conductivity,[19,20] which is opposite to the n-type behavior of SnO_2. This is an interesting finding because wide band gap semiconductor oxides with high p-type conductivity are not common.

The phase diagram for the Sn-O system[21] indicates that SnO is a thermodynamically unstable phase. In fact, studies of SnO discs have shown this material changing into the SnO_2 phase when heat-treated after a decomposition process with the Sn_3O_4 intermediary phase,[15] and that during the phase transition the discs' morphology changes from monocrystalline to polycrystalline. Nevertheless, to date it is not known what occurs during the transition from the SnO phase to the SnO_2 phase in SnO nanobelts.

The main goal of the present work was to study the thermal stability of nanobelts grown in the orthorhombic SnO phase, as well as the main phase transition mechanisms. The morphological and structural changes of these nanobelts after the phase transition were also investigated and are discussed in detail.

Experimental Procedures

The SnO nanobelts were obtained by the carbothermal reduction process, using SnO_2 powder mixed with carbon black as starting materials. After synthesization, a grayish-black wool-like material was collected downstream, which was composed of SnO nanobelts and discs. Details regarding this synthesis are given elsewhere.[17]

The thermal stability and phase transition of nanobelts in the grayish-black material were studied by differential scanning calorimetry (DSC; Netzsch, model 404 C). The DSC analyses were performed at 800 °C for 1 h, at a heating and cooling rate of 5 °C min^{-1}, in oxygen or synthetic air or argon atmosphere, and a gas flux of 50 cm^3 min^{-1}.

After the heat treatment, the materials were structurally characterized by X-ray diffraction (XRD; Siemens, model D-5000) using CuK_α radiation. For the XRD measurements, the samples were placed in a metallic aluminum sample holder, and analyses were performed between 10 and 75 degrees, which is the range in which most tin oxide peaks occur. A field emission scanning electron microscope (FE-SEM; Zeiss, model Supra 35) was used for the microstructural characterization, and a high resolution transmission electron microscope (TEM; Jeol, model 3010, URP) operating at 300 kV was used for the structural and microstructural characterizations. To prepare the samples for electron microscopy, the materials were placed in an isopropanol medium and treated ultrasonically to aid their dispersion. A drop of the suspension was deposited onto carbon-coated copper grids. The samples were dried in air and at room temperature.

Results and Discussion

After the heat treatments in the DSC furnace, the grayish-black wool-like material turned white, independently of the atmosphere used (oxygen or synthetic air or argon). Figure 1a,b shows the X-ray diffraction pattern of the white material obtained in oxygen and argon atmospheres, respectively. The Al peaks in Figure 1 were due to the sample holder used in the measurements, and the other peaks were indexed as SnO_2. The peaks labeled (+) were identified as rutile SnO_2 structure (JCPDS No. 41.1445), while those labeled (○) indicated the

* To whom correspondence should be addressed. Tel: 55 18 3743-1029; fax: 55 18 3742-4868; e-mail: orlandi@dfq.feis.unesp.br.
† Departamento de Física e Química, Universidade Estadual Paulista.
‡ Laboratório Nacional de Luz Síncrotron.
§ Universidade Federal de São Carlos.
△ Instituto de Química, Universidade Estadual Paulista.

10.1021/cg7009379 CCC: $40.75
Published on Web 02/15/2008

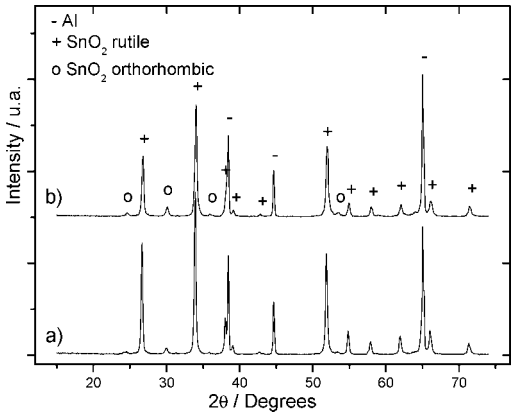

Figure 1. X-ray diffraction pattern of the gray-black wool-like material after heat treatment in oxygen atmosphere (a) and argon atmosphere (b).

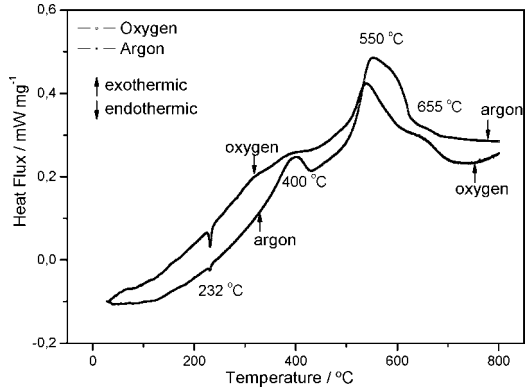

Figure 2. Differential scanning calorimetry measurements of the gray-black wool-like material in oxygen and argon atmosphere.

more intense peaks of orthorhombic SnO_2 structure (JCPDS No. 29.1484). The relative intensities of the peaks revealed that the presence of the rutile-type structure was predominant. The same result was observed for the sample treated in synthetic air. In their study of phase transition in SnO discs, Dai et al.[15] did not observe the orthorhombic SnO_2 phase, although they identified an extra peak at $2\theta = 29.8°$, which was attributed to residual SnO.

It is interesting to note that the same final phase was obtained after heat treatments in oxidizing or inert atmospheres. The reason for this result is that the phase transition from SnO to SnO_2 is a decomposition process.[15,21] In the absence of oxygen, the following chemical decomposition reaction occurs at 400 °C:[21]

$$2SnO_{(s)} \rightarrow SnO_{2(s)} + Sn°_{(l)} \quad (1)$$

The following chemical reactions occur in room atmosphere in the range of 400−1040 °C:[15,21]

$$4SnO_{(s)} \rightarrow Sn_3O_{4(s)} + Sn°_{(l)} \quad (2)$$

$$Sn_3O_4 \rightarrow 2SnO_{2(s)} + Sn°_{(l)} \quad (3)$$

in which the subscripts s and l mean solid and liquid, respectively.

The Sn_3O_4 phase is absent from Figure 1 because it is an intermediary byproduct of the decomposition process, and the XRD analyses were done after the entire heat treatment process.

Figure 2 shows the DSC measurements of the grayish-black wool-like material in oxygen and argon atmospheres. The

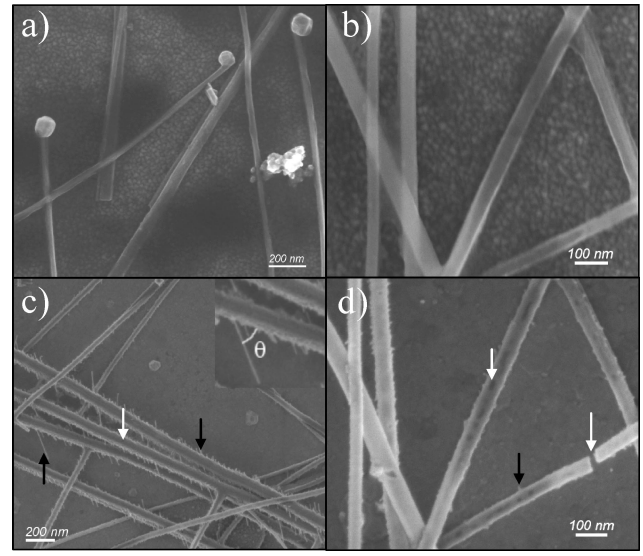

Figure 3. (a, b) SEM images of the as-synthesized nanobelts. (c, d) SEM images of the nanobelts after heat treatment in oxygen atmosphere. The inset in Figure 3c shows the angle θ between the nanofibers and the belt edge, which is about 50°. Images b and d show the same region before and after the heat treatment.

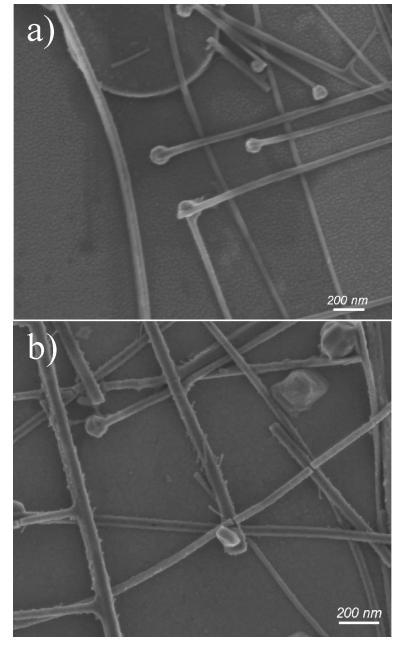

Figure 4. SEM images before (a) and after (b) heat treatment in synthetic air atmosphere.

endothermic peak at 232 °C was due to melting of the metallic tin spheres existing at the extremity of the belts.[17] The sample treated in argon showed a clear exothermic peak at 400 °C, which is evidence that reaction 1 occurred in the absence of oxygen. However, some SnO nanobelts may not decompose directly by reaction 1, and the broad peak at 550 °C and the one at 655 °C were ascribed to reactions 2 and 3, respectively, even in argon atmosphere. For the sample heat-treated in oxygen atmosphere, the peak at 400 °C is not evident, but it displays two peaks, one at 540 °C and other at 650 °C, which were associated with reactions 2 and 3. It is noteworthy mentioning that reactions 1–3 yield metallic tin; nonetheless, no peak corresponding to solidification of metallic tin was observed

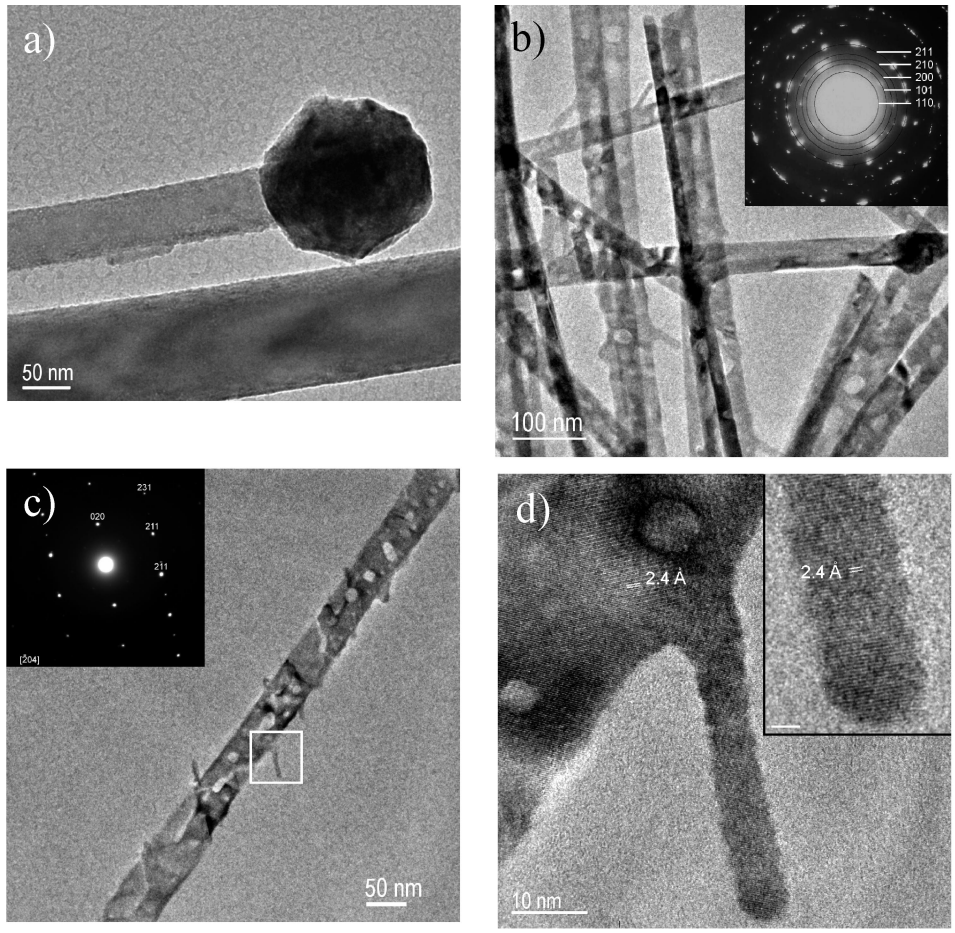

Figure 5. (a) Nanobelts of the as-synthesized material before heat treatment. (b) Bright field TEM image of a group of nanobelts after heat treatment in oxygen atmosphere. The inset shows the SAED picture of the belts presenting a polycrystalline-like pattern. (c) TEM image of a typical nanobelt after the same heat treatment. The monocrystalline characteristic of individual belt is showed in the SAED pattern of inset. (d) HRTEM image of the white square marked in c). The inset shows an enlarged view of the tip of the nanofiber (the scale bar of inset is 2 nm).

during the DSC cooling measurements (not shown here). This result is explained as follows.

Figure 3 shows SEM images of nanobelts before and after the heat treatment in oxygen atmosphere. Two main changes were clearly visible in the morphology of the nanobelts after the heat treatment. The first change observed was the formation of superficial *holes* along the belt (white arrows) and some cracked nanobelts (Figure 3d), while the second one was the appearance of nanofibers or dendrites (hereinafter called nanofibers) at the belts' edges (black arrows). It is interesting to note that the fibers always grew parallel to each other, independent of the position along the belt, and that the angle θ between them and the belt edge (inset in Figure 3c) was always at about 50°. The sample treated in synthetic air showed the same result as it did in oxygen atmosphere, indicated in Figure 4.

Figure 5a,b shows a bright field TEM image of nanobelts before and after heat treatment in oxygen atmosphere, respectively. In Figure 5b, as can be seen by mass contrast, some regions in the middle of the belt are thinner than the edges, forming cavity-like structures along the belt's surface, which contrasts with the flat and clean surface of belts before heat treatment.[17] Inserted in this figure is the selected area electron diffraction (SAED) picture of a group of nanobelts, revealing a polycrystalline-like pattern. The SAED was indexed as rutile SnO_2 structure, which proves that belts transform to cassiterite phase after heat treatment. Figure 5c presents one typical nanobelt after heat treatment that possesses nanofibers at the edges and a thinner middle in some regions. Using SAED

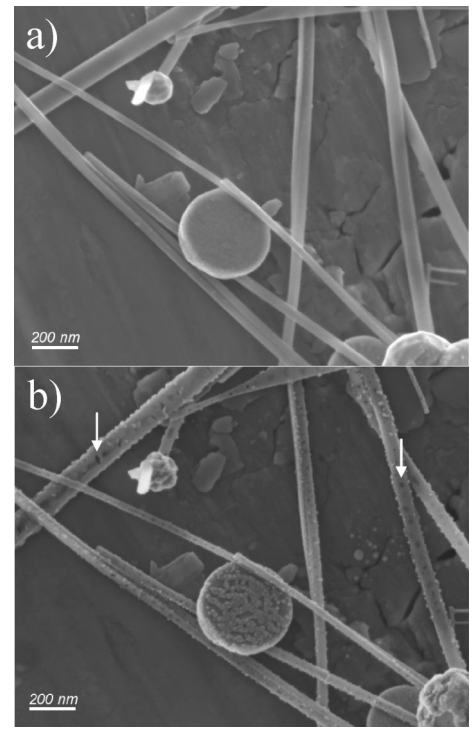

Figure 6. SEM images of nanobelts before (a) and after (b) heat treatment in argon atmosphere.

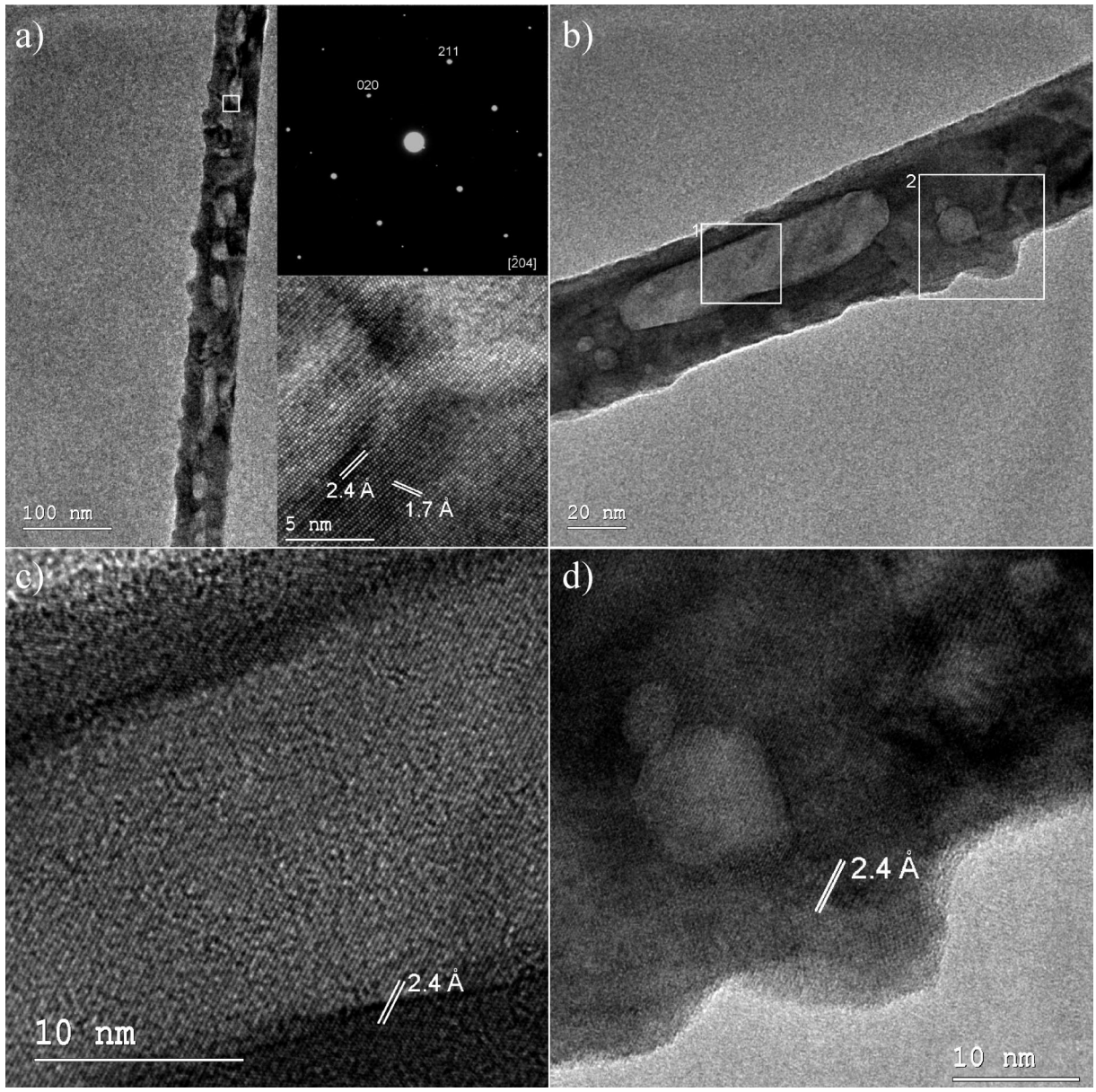

Figure 7. (a) Bright field TEM image of a nanobelt after heat treatment in argon atmosphere. The upper inset shows the SAED pattern of a nanobelt and the lower one shows the HRTEM image of the white square market in the nanobelt. (b) TEM image of another nanobelt. (c) HRTEM image of the central region of the image (b) (white square labeled 1), and (d) HRTEM image of the edge region of the image (b) (white square labeled 2).

characterization, it was observed that each belt is monocrystalline, as observed in the inset of Figure 5c. The SAED was indexed as [$\bar{2}$04] zone axis of rutile SnO_2 structure.

Combining the SAED with the high resolution transmission electron microscopy (HRTEM) image of Figure 5d, one can see that the fibers grew in the <010> direction of the rutile structure. Once the growth of nanofibers occurs during a heat treatment the process should be thermodynamically controlled. In fact, for rutile SnO_2, the <010> growth direction with the (100) and (001) planes as facets is thermodynamically favorable ($\Delta G = -1.84$ J m^{-2}).[22] It is also the axis that a pyramid is formed by (110) and (101) planes, which are closely packed planes for this structure, as required for fibers growth.[22,23] Thus, the <010> direction complies with the thermodynamic requirements for the fiber growth direction. On the basis of the SAED pattern, the belts grew in the plane (221), which is about 51° from the (020) plane, and these results are evidence that there are no crystallographic connections between the belts before and after the heat treatment. It is worth mentioning that, although the diffraction of the (010) plane is kinematically prohibitive for space group *P*42/*mnm* (136), it is possible to see weak points relating to this plane in SAED, due to the dynamical effects of electron diffraction.[25]

Unlike the results presented previously, the sample heat-treated in argon atmosphere displayed particles instead of nanofibers at the nanobelt surface, as shown in Figure 6, although cavity-like structures were still present along the belts (white arrows). Figure 7a,b shows bright field TEM images of typical belts after heat treatment in argon atmosphere, revealing superficial particles and cavities. These belts were also monocrystalline, as indicated by the SAED pattern of Figure 7a, and they are also oriented in the [$\bar{2}$04] zone axis of the rutile structure. Here, again, one can see weak diffraction points of the (010) plane. Using HRTEM characterization, Figure 7c, it was possible to observe that the so-called cavities were simply thinner regions of the belt, and they presented the same

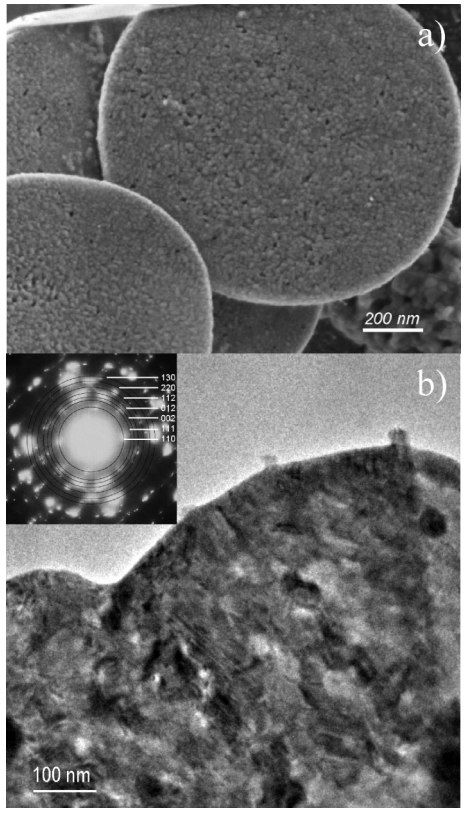

Figure 8. (a) SEM and (b) TEM and SAED image of discs after heat treatment in oxygen atmosphere, showing a polycrystalline morphology.

crystallographic orientation of the whole belt without any dislocation or other planar defects in the regions surrounding the cavities. For the superficial particles, HRTEM images showed they are also in the same crystallographic orientation of the belt (Figure 7d), which is evidence that particles are not in a metallic tin phase, as predicted by reaction 1.

Figure 8 shows SEM and TEM images of discs after heat treatment in oxygen atmosphere, demonstrating that the disk surface is rugose when compared with the flat and clean surfaces of the original discs.[17] The SAED pattern of disk present a polycrystalline characteristic, hence providing evidence that discs change from monocrystalline to polycrystalline array during the phase transition, which is in agreement with Dai's findings.[15] However, by indexing the SAED pattern it was found that discs transform to the orthorhombic structure of SnO_2, whose more intense planes are illustrated in the SAED, with this result explaining the peaks of this phase observed in XRD diffractogram. This result differs from that obtained by Dai et al., who reported that tetragonal SnO discs transform to rutile SnO_2 after heat treatment.[15] At present, it is not yet fully understood why nanobelts transform to rutile SnO_2 and discs to orthorhombic SnO_2 during the phase transition, but it might very well be related to their different initial structures; SnO nanobelts grew in an orthorhombic structure, and SnO discs grew in a tetragonal structure.

The formation of cavities and cracks in nanobelts after heat treatments is attributed to two mechanisms that occur during the decomposition process, that is, phase separation and cell volume change. During phase transition, Sn° and SnO_2 phases are formed in the decomposition process, and since these phases are not miscible in this temperature range,[21] the liquid metallic tin migrates out of the solid tin dioxide, leaving cavities along the belts. Moreover, during the decomposition process, the cell volume is reduced by about 22% from orthorhombic SnO to rutile SnO_2. This cell volume reduction causes stress in the belts, which can even break it, but each part of the belt remains monocrystalline. The large surface area to volume ratio of the belts is the main reason behind this effect, since superficial atoms have higher energy than bulk atoms, and higher diffusivity allows for structural rearrangements in the belts. In the case of tetragonal SnO discs, also present in the grayish-black material,[17] which have a low surface area to volume ratio, they change from monocrystalline discs to polycrystalline discs during the phase transition from SnO to SnO_2 (Figure 8 and ref 15).

The following mechanism is proposed to explain the nanofibers formation in oxygen atmosphere and the superficial particles in argon atmosphere. Metallic tin is formed during the decomposition process in the presence of oxygen, as predicted by reactions 2 and 3. This metallic tin should be in liquid form and outside of the tin oxide matrix, preferably located at a high energy position of the nanobelts surface, that is, at the belt edges. Because of the large amount of oxygen available in the furnace in pure oxygen and synthetic air atmospheres, it is proposed that metallic tin can become supersaturated by oxygen, allowing for the growth of tin oxide fibers by a vapor−liquid−solid (VLS) process. This process can be described as an autocatalytic VLS process since the metallic tin particles were generated during the decomposition process. Although this growth mechanism is the same as that proposed for the growth of SnO dendrites in some original SnO nanobelts,[17] the whole process is different once the metallic tin particles originate from different sources in each case. In the former, the source was the synthesis atmosphere, while the latter originated from the nanobelt itself, due to the decomposition process. This growth mechanism explains why no exothermic peak arising from the solidification of metallic tin was observed during DSC cooling measurements in oxygen and synthetic air atmospheres.

On the basis of the proposed growth mechanism, no fiber growth is expected to occur if the heat treatment atmosphere does not have available oxygen to supersaturate the metallic tin particles, as for instance, in an argon atmosphere. In this case, only metallic tin particles should appear on the nanobelts' surfaces. The results showed the presence of superficial particles, but in the SnO_2 phase, and no metallic tin peaks were revealed by XRD and DSC cooling measurements. This was attributed to the presence of residual oxygen in the furnace, which can react with the small metallic tin particles to form tin oxide particles (Figures 6 and 7). Therefore, it must have been only residual oxygen, since it was insufficient to supersaturate the particles to produce the growth of nanofibers.

Tin oxide is an important material with promising technological applications in devices that require large surface areas. The SnO_2 nanobelts generated by decomposition from SnO should increase the surface area to volume ratio due to the presence of nanofibers at its edge. On that account, this may be an interesting way to synthesize such material. However, further studies are necessary to study the electrical and optical properties of these belts.

Conclusions

The thermal stability of orthorhombic tin monoxide nanobelts was studied, and the results confirmed it is a thermodynamically unstable phase of the Sn-O system. Seeing that the phase transition is a decomposition process, the SnO_2 phase is obtained independently of the heat treatment atmosphere. Nanobelts undergo two major morphological changes during the decom-

position process: the formation of cavities along the surface of the belts, and formation of nanofibers or particles on the surface of the belts. The formation of cavities was attributed to phase separation and cell volume reduction during the phase transformation process. The growth of fibers was related directly to oxygen in the heat treatment atmosphere, and growth occurs autocatalytically. The nanofibers grew in the <010> direction of the SnO_2 rutile structure, which is a thermodynamically favorable direction if the facet planes are (100) and (001). The formation of superficial particles was attributed to metallic tin resulting from the decomposition process in argon atmosphere. Nanofibers growth and cavities should increase the nanobelts' surface area, which may be of technological interest.

Acknowledgment. The financial backing of the Brazilian agencies FUNDUNESP, FAPESP, and CNPq are gratefully acknowledged. The TEM facilities were provided by the LME-LNLS (National Laboratory of Synchrotron Light), Campinas, SP, Brazil.

References

(1) Lee, T. S.; Wang, N.; Zhang, Y. F.; Tang, Y. H. *MRS Bull.* **1999**, *24*, 36.
(2) Yang, P. D.; Lieber, C. M. *J. Mater. Res.* **1997**, *12*, 2981.
(3) Leite, E. R.; Vila, C.; Bettini, J.; Longo, J. *J. Phys. Chem B* **2006**, *110*, 18088.
(4) Manna, L.; Scher, E. C.; Alivisatos, A. P. *J. Am. Chem. Soc.* **2000**, *122*, 12700.
(5) Sapp, S. A.; Mitchell, D. T.; Martin, C. R. *Chem. Mater.* **1999**, *11*, 1183.
(6) Li, M.; Schnablegger, H.; Mann, S. *Nature* **1999**, *10*, 1358.
(7) Duan, X. F.; Lieber, C. M. *Adv. Mater.* **2000**, *12*, 298.
(8) Ginley, D. S.; bright, C. *MRS Bull.* **2000**, *25*, 15.
(9) Fagan, F. G.; Amarakoon, V. R. W. *Am. Ceram. Soc. Bull.* **1993**, *72*, 119.
(10) Zhang, Y.; Kolmakov, A.; Lilach, Y.; Moskovits, M. *J. Phys. Chem. B* **2005**, *109*, 1923.
(11) Vayssieres, L.; Graetzel, M. *Angew. Chem., Int. Ed.* **2004**, *43*, 3666.
(12) Dai, Z. R.; Pan, Z. W.; Wang, Z. L. *Solid State Commun.* **2001**, *118*, 351.
(13) Hu, J. Q.; Ma, X. L.; Shang, N. G.; Xie, Z. Y.; Wong, N. B.; Lee, C. S.; Lee, S. T. *J. Phys. Chem. B* **2002**, *106*, 3823.
(14) Leite, E. R.; Gomes, J. W.; Oliveira, M. M.; Lee, E. J. H.; Longo, E.; Varela, J. A.; Paskocimas, C. A.; Boschi, T. M., Jr.; Pizani, P. S., Jr; Soares, P. C. *J. Nanosci. Nanotechnol.* **2002**, *2*, 125.
(15) Dai, Z. R.; Pan, Z. W.; Wang, Z. L. *J. Am. Chem. Soc.* **2002**, *124*, 8673.
(16) Z. L Wang, Z. L.; Pan, Z. W. *Adv. Mater.* **2002**, *14*, 1029.
(17) Orlandi, M. O.; Leite, E. R.; Aguiar, R.; Bettini, J.; Longo, E. *J. Phys. Chem. B* **2006**, *110*, 6621.
(18) Domashevskaya, E. P.; Ryabtsev, S. V.; Yurakov, Yu.A.; Chuvenkova, O. A.; Kashkarov, V. M.; Turishchev, S.Yu.; Kushev, S. B.; Lukin, A. N. *Thin Solid Films* **2007**, *515*, 6350.
(19) Pan, X. Q.; Fu, L. *J. Electroceram.* **2001**, *7*, 35.
(20) Togo, A.; Oba, F.; Tanaka, I.; Tatsumi, K. *Phys. Rev. B* **2006**, *74*, 195128.
(21) Samsonov, G. V. *The Oxide Handbook*; Plenum Press: New York, 1973.
(22) Beltran, A.; Andres, J.; Longo, E.; Leite, E. R. *Appl. Phys. Lett.* **2003**, *83*, 635.
(23) Weinberg, F.; Chalmers, B. *Can. J. Phys.* **1952**, *30*, 488.
(24) Bolling, G. F.; Tiller, W. A. *J. Appl. Phys.* **1961**, *32*, 2587.
(25) Williams, D. B.; Carter, C. B. *Transmission Electron Microscopy*; Springer: New York, 1996.

CG7009379